

---

# Subgraph Neural Networks

---

**Emily Alsentzer\***  
Harvard University, MIT  
emilya@mit.edu

**Samuel G. Finlayson\***  
Harvard University, MIT  
sgfin@mit.edu

**Michelle M. Li**  
Harvard University  
michelleli@g.harvard.edu

**Marinka Zitnik**  
Harvard University  
marinka@hms.harvard.edu

## Abstract

Deep learning methods for graphs achieve remarkable performance on many node-level and graph-level prediction tasks. However, despite the proliferation of the methods and their success, prevailing Graph Neural Networks (GNNs) neglect subgraphs, rendering subgraph prediction tasks challenging to tackle in many impactful applications. Further, subgraph prediction tasks present several unique challenges: subgraphs can have non-trivial internal topology, but also carry a notion of position and external connectivity information relative to the underlying graph in which they exist. Here, we introduce SUBGNN, a subgraph neural network to learn disentangled subgraph representations. We propose a novel subgraph routing mechanism that propagates neural messages between the subgraph’s components and randomly sampled anchor patches from the underlying graph, yielding highly accurate subgraph representations. SUBGNN specifies three channels, each designed to capture a distinct aspect of subgraph topology, and we provide empirical evidence that the channels encode their intended properties. We design a series of new synthetic and real-world subgraph datasets. Empirical results for subgraph classification on eight datasets show that SUBGNN achieves considerable performance gains, outperforming strong baseline methods, including node-level and graph-level GNNs, by 19.8% over the strongest baseline. SUBGNN performs exceptionally well on challenging biomedical datasets where subgraphs have complex topology and even comprise multiple disconnected components.

## 1 Introduction

Deep learning on graphs and Graph Neural Networks (GNNs), in particular, have emerged as the dominant paradigm for learning representations on graphs [66, 81, 23]. These methods condense neighborhood connectivity patterns into low-dimensional embeddings that can be used for a variety of downstream prediction tasks. While graph representation learning has made tremendous progress in recent years [20, 84], prevailing methods focus on learning useful representations for nodes [25, 68], edges [21, 37] or entire graphs [6, 27].

Graph-level representations provide an overarching view of the graphs, but at the loss of some finer local structure. In contrast, node-level representations focus instead on the preservation of the local topological structure (potentially to the detriment of the big picture). It is unclear if these methods can generate powerful representations for subgraphs and effectively capture the unique topology of subgraphs. Despite the popularity and importance of subgraphs for machine learning [77, 13, 78], there is still limited research on subgraph prediction [41], *i.e.*, to predict if a particular subgraph has

---

\*Contributed Equally.

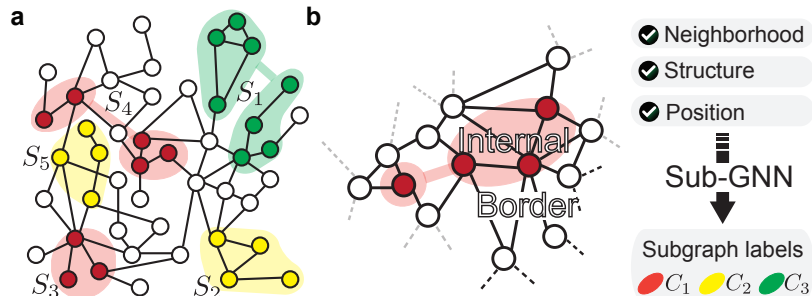


Figure 1: **a.** Shown is graph  $G$  in which nodes explicitly state their group memberships, resulting in intricate subgraph structures,  $\mathcal{S} = \{S_1, \dots, S_5\}$ . Subgraphs  $S_2, S_3$  and  $S_5$  comprise single connected components in  $G$  whereas subgraphs  $S_1$  and  $S_4$  each form two isolated components. Colors indicate subgraph labels,  $\mathcal{C} = \{C_1, C_2, C_3\}$ . **b.** We investigate the problem of predicting subgraph properties  $\mathcal{C}$  by learning subgraph representations that recognize and disentangle the heterogeneous properties of subgraphs (*i.e.*, neighborhood, structure, and position) and how they relate to underlying  $G$  (*i.e.*, internal connectivity and border structure of the edge volume that points outside of the subgraph).

a particular property of interest (Figure 1a). This can be, in part, because subgraphs are incredibly challenging structures from the topological standpoint (Figure 1b). (1) Subgraphs require that we make joint predictions over larger structures of varying sizes—the challenge is how to represent subgraphs that do not correspond to enclosing  $k$ -hop neighborhoods of nodes and can even comprise of multiple disparate components that are far apart from each other in the graph. (2) Subgraphs contain rich higher-order connectivity patterns, both internally among member nodes as well as externally through interactions between the member nodes and the rest of the graph—the challenge is how to inject information about border and external subgraph structure into the GNN’s neural message passing. (3) Subgraphs can be localized and reside in one region of the graph or can be distributed across multiple local neighborhoods—the challenge is how to effectively learn about subgraph positions within the underlying graph in which they are defined. (4) Finally, subgraph datasets give rise to unavoidable dependencies that emerge from subgraphs sharing edges and non-edges—the challenge is how to incorporate these dependencies into the model architecture while still being able to take feature information into account and facilitate inductive reasoning.

**Present work.** Here, we introduce SUBGNN<sup>2</sup> (Figure 2), a novel graph neural network for subgraph prediction that addresses all of the challenges above. Unlike current prediction problems that are defined on individual nodes, pairwise relations, or entire graphs, our task here is to make predictions for subgraphs. To the best of our knowledge, SUBGNN is the only representation learning method designed for general subgraph classification. While [41] performs prediction on small (3-4 nodes), fixed-size subgraphs, SUBGNN operates on larger subgraphs with varying sizes and multiple connected components. SUBGNN’s core principle is to propagate messages at the subgraph level, via three property-aware channels that capture position, neighborhood, and structure. Further, SUBGNN is inductive: it can operate on new subgraphs in unseen portions of the graph.

Experiments on eight datasets show that SUBGNN outperforms baselines by an average of 77.4% on synthetic datasets and 125.2% on real-world datasets. Further, SUBGNN improves the strongest baseline by 19.8%. As an example, on a network of phenotypes where subgraphs represent symptoms of a disease, our method is able to distinguish between 10 subcategories of monogenic neurological disorders. We also find that several naive generalizations of node-level and graph-level GNNs have poor performance. This finding is especially relevant as these generalizations are popular in practical applications, yet they cannot fully realize the potential of neural message-passing for subgraph prediction, as evidenced by our experiments. For example, we find that a popular node-level approach, which represents subgraphs with virtual nodes (*i.e.*, meta nodes) and then uses an attention-based GNN (*e.g.*, GAT [62]) to train a node classifier, performs poorly in a variety of settings.

Finally, we design a suite of synthetic subgraph benchmarks that are uniquely suited for evaluating aspects of subgraph topology. We also provide four new and original real-world datasets from

<sup>2</sup>Code and datasets are available at <https://github.com/mims-harvard/SubGNN>.

biological, medical, and social domains to practically test the new algorithms. Each dataset consists of an underlying graph overlaid with a large number of subgraphs whose labels we need to predict.

## 2 Related Work

We proceed by reviewing major threads of research relevant for subgraph representation learning.

**Subgraph embeddings and prediction.** A few recent works learn representations of small, localized subgraphs. [10] encodes the subgraph of entities connected to the candidate answer entity in a knowledge graph for question answering, and [41] encodes 3-node or 4-node subgraphs for subgraph evolution prediction. In contrast, SUBGNN can learn representations for large, variable-size subgraphs that can be distributed throughout the graph.

**Subgraph extraction and network community detection.** The topology of border structure has been extensively examined in the context of community detection [71, 46, 67] (also known as module detection and graph clustering), highlighting its importance for network science [8, 47]. However, community detection, motif counting, and embedding methods for subgraph extraction and kernel-based similarity estimation [53, 58, 74, 63, 30, 15, 2, 35] are fundamentally different from SUBGNN. These methods search for groups of nodes that are well-connected internally while being relatively well-separated from the rest of the graph and typically limited to individual connected components. In contrast, SUBGNN is a subgraph prediction framework that reasons over a given set of subgraphs.

**Learning representations of higher-order structures, ego nets, and enclosing subgraphs.** Hypergraph neural networks [82] and their variants [54, 18, 79, 45, 80] have become a popular approach for learning on hypergraph-structured data. These methods use the spectral theory of hypergraphs [70] or clique expansion [1, 29, 31] to formulate higher-order message passing, where nodes receive latent representations from their immediate (one-hop) neighbors and from further  $N$ -hop neighbors at every message passing step. Recent studies, *e.g.*, [76, 44, 64, 10], also learn representations for permutation-invariant functions of sequences (or multiset functions [40]). These methods typically express permutation-invariant functions as the average of permutation-sensitive functions applied to all reorderings of the input sequence. While this approach allows for pooling operators that are invariant to the ordering of nodes, it does not account for rich subgraph dependencies, such as when subgraphs share edges and have many connections to the rest of the graph.

**Subgraphs and patches in GNNs.** Subgraph structure is key for numerous graph-related tasks [61, 16, 73]. For example, Patchy-San [49] uses local receptive fields to extract useful features from graphs. Ego-CNN uses ego graphs to find critical structures [60]. SEAL [78] develops a theory showing that enclosing subgraphs are sufficient for link prediction. Building on this evidence, GraIL [59] extracts local subgraphs induced by nodes occurring on the shortest paths between the target nodes and uses them for inducing logical rules. Cluster-GCN [13], Ripple walks [5], and GraphSAINT [77] use subgraphs to design more efficient and scalable algorithms for training deep and large GNNs. While these methods use substructures to make GNN architectures more efficient or improve performance on node and edge prediction tasks, none of the methods consider prediction on subgraphs.

## 3 Formulating Subgraph Prediction

Let  $G = (V, E)$  denote a graph comprised of a set of edges  $E$  and nodes  $V$ . While we focus on undirected graphs, it is straightforward to extend this work to directed graphs.  $S = (V', E')$  is a subgraph of  $G$  if  $V' \subseteq V$  and  $E' \subseteq E$ . Each subgraph  $S$  has a label  $y_S$  and may consist of multiple connected components,  $S^{(C)}$ , which are defined as a set of nodes in  $S$  such that each pair of nodes is connected by a path (*e.g.*, see Figure 1). Importantly, the number and size of the subgraphs are bounded by, but do not directly depend on, the number of nodes in the graph  $G$ .

**Background on Graph Neural Networks.** Many graph neural networks, including ours, can be formulated as message passing networks (MPN) [7, 65, 83]. Message-passing networks are defined by three functions, MSG, AGG, and UPDATE, which are used to propagate signals between elements of the network and update their respective embeddings. Typically, these functions are defined to operate at the node level, propagating messages to a node  $v_i$  from the nodes in its neighborhood  $\mathcal{N}_{v_i}$ . In this typical context, a message between a pair of nodes  $(v_i, v_j)$  at layer  $l$  is defined as a function of the hidden representations of the nodes  $\mathbf{h}_i^{l-1}$  and  $\mathbf{h}_j^{l-1}$  from the previous layer:  $m_{ij}^l = \text{MSG}(\mathbf{h}_i^{l-1}, \mathbf{h}_j^{l-1})$ .

In AGG, messages from  $\mathcal{N}_{v_i}$  are aggregated and combined with  $\mathbf{h}_i^{l-1}$  to produce  $v_i$ 's representation for layer  $l$  in UPDATE. Many extensions of the canonical message passing framework have been proposed [7, 62, 13, 22], e.g., [75] passes messages from a shared set of anchor nodes rather than a strict neighborhood, to allow node embeddings to capture global position.

### 3.1 SUBGNN: Problem Formulation

**Problem (Subgraph Representations and Property Prediction).** Given subgraphs  $\mathcal{S} = \{S_1, S_2, \dots, S_n\}$ , SUBGNN specifies a neural message passing architecture  $E_S$  that generates a  $d_s$ -dimensional subgraph representation  $\mathbf{z}_S \in \mathbb{R}^{d_s}$  for every subgraph  $S \in \mathcal{S}$ . SUBGNN uses the representations to learn a subgraph classifier  $f : \mathcal{S} \rightarrow \{1, 2, \dots, C\}$  for subgraph labels  $f(S) = \hat{y}_S$ .

Note that while this paper focuses on the subgraph classification task, the methods we propose entail learning an embedding function  $E_S : \mathcal{S} \rightarrow \mathbb{R}^{d_s}$  that maps each subgraph to a low-dimensional representation that captures the key aspects of subgraph topology necessary for prediction. All the techniques that we introduce to learn  $E_S$  can be extended without loss of generality to other supervised, unsupervised, or self-supervised tasks involving subgraphs.

In this work, we define message passing functions that operate at the *subgraph* level. This allows us to explicitly capture aspects of subgraph representation that do not apply to nodes or whole graphs. In particular, messages are propagated to each connected component in the subgraph, allowing us to build meaningful representations of subgraphs with multiple distinct connected components.

**SUBGNN: Properties of subgraph topology.** Subgraph representation learning requires models to encode network properties that are not necessarily defined for either nodes or graphs. Subgraphs have non-trivial internal structure, border connectivity, and notions of neighborhood and position relative to the rest of the graph. Intuitively, our goal is to learn a representation of each subgraph  $S_i$  such that the likelihood of preserving certain properties of the subgraph is maximized in the embedding space. Here we provide a framework of six properties of subgraph structure that are key for learning powerful subgraph representations (Table 1).

Table 1: Six properties of subgraph topology in SUBGNN. Internal nodes correspond to nodes within the subgraph  $S_i$  in graph  $G$ , and border nodes correspond to nodes within the  $k$ -hop neighborhood of any node in  $S_i$ . See also Figure 1.

SUBGNN Channel	SUBGNN Subchannel	
	Internal (I)	Border (B)
Position (P)	Distance between $S_i$ 's components	Distance between $S_i$ and rest of $G$
Neighborhood (N)	Identity of $S_i$ 's internal nodes	Identity of $S_i$ 's border nodes
Structure (S)	Internal connectivity of $S_i$	Border connectivity of $S_i$

**1) Position.** Two notions of position may be defined for subgraphs. The first, *border position*, refers to its distance to the rest of  $G$ ; this is directly analogous to node position, which can distinguish nodes with isomorphic neighborhoods [75]. The second, *internal position*, captures the relative distance between components within the subgraph.

**2) Neighborhood.** Subgraphs extend the notion of a node's neighborhood to include both internal and external elements. *Border neighborhood*, as with nodes, is defined as the set of nodes within  $k$  hops of any node in  $S$ . Each connected component in a subgraph will have its own border neighborhood. Subgraphs also have a non-trivial *internal neighborhood*, which can vary in size and position.

**3) Structure.** The connectivity of subgraphs is also non-trivial. A subgraph's *internal structure* is defined as the internal connectivity of each component. Simultaneously, subgraphs have a *border structure*, defined by edges connecting internal nodes to the border neighborhood.

We expect that capturing each of these properties will be crucial for learning useful subgraph representations, with the relative importance of these properties determined by the downstream task.

## 4 SUBGNN: SUBGRAPH NEURAL NETWORK

Next, we describe SUBGNN, our approach to subgraph classification, which is designed to learn representations that can capture the six aspects of subgraph structure from Table 1. SUBGNN

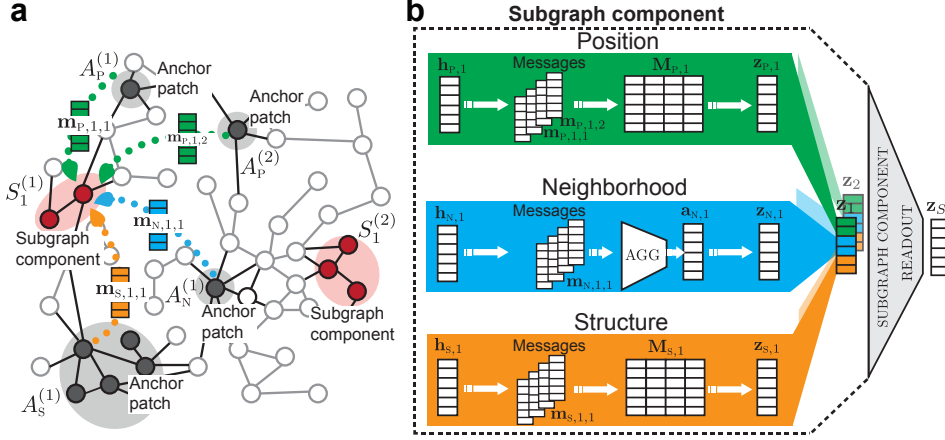


Figure 2: SUBGNN architecture. **a.** Property-specific messages  $\text{MSG}_X^{A \rightarrow S}$  are propagated from anchor patches  $A_x$  to components of subgraph  $S$ . Here,  $\mathbf{m}_{x,c,i}$  denotes property- $x$  message from  $i$ -th anchor patch  $A_x^{(i)}$  to  $c$ -th component  $S^{(c)}$ . **b.** SUBGNN specifies three channels, which are each designed to capture a distinct subgraph property. Channel outputs  $\mathbf{z}_x$  are concatenated to produce a final subgraph representation  $\mathbf{z}_S$ .

learns representations of subgraphs in a hierarchical fashion, by propagating neural messages from anchor patches to subgraph components and aggregating the resultant representations into a final subgraph embedding (Figure 2a). Message-passing for each connected component takes place in independent position, neighborhood, and structure channels, each explicitly optimized to encode a distinct subgraph property (Figure 2b). The messages are sent from anchor patches sampled from throughout the graph and weighted by a property-specific similarity function. This approach is modular, extensible, and can be customized based on knowledge of the downstream task.

#### 4.1 Subgraph-Level Message Passing

The core of our approach is a message passing framework, as described in Table 1. SUBGNN specifies a novel aggregation scheme that is defined at the level of subgraph components. SUBGNN specifies how to propagate neural messages from a set of anchor patches to subgraph components and, eventually, to entire subgraphs, resulting in subgraph representations that capture distinct properties of subgraph topology (Table 1).

Anchor patches  $\mathcal{A}_x = \{A_x^{(1)}, \dots, A_x^{(n_A)}\}$  are subgraphs, which we randomly sample from  $G$  in a channel-specific manner, resulting in anchor patches  $\mathcal{A}_p$ ,  $\mathcal{A}_n$ , and  $\mathcal{A}_s$  for each of three SUBGNN’s channels, position, structure, and neighborhood, respectively. We define the message from anchor patch  $A_x$  to subgraph component  $S^{(c)}$  as follows:

$$\text{MSG}_X^{A \rightarrow S} = \gamma_x(S^{(c)}, A_x) \cdot \mathbf{a}_x \quad (1)$$

where  $x$  is the channel,  $\gamma_x$  a similarity function between the component  $S^{(c)}$  and the anchor patch  $A_x$ , and  $\mathbf{a}_x$  is the learned representation of  $A_x$ . Similarity function  $\gamma_x$  is any learned or pre-specified similarity measure quantifying the relevance of an anchor patch to a subgraph. These messages are then transformed into order-invariant hidden representation  $\mathbf{h}_{x,c}$  and subgraph component  $S^{(c)}$  as:

$$\begin{aligned} \mathbf{g}_{x,c} &= \text{AGG}_M(\{\text{MSG}_X^{A_x \rightarrow S^{(c)}} \mid \forall A_x \in \mathcal{A}_x\}), \\ \mathbf{h}_{x,c} &\leftarrow \sigma(\mathbf{W}_x \cdot [\mathbf{g}_{x,c}; \mathbf{h}_{x,c}]), \end{aligned} \quad (2)$$

where  $\mathbf{W}_x$  is a layer-wise learnable weight matrix for channel  $x$ ,  $\sigma$  is a non-linear activation function,  $\text{AGG}_M$  is an aggregation function that operates over messages, and  $\mathbf{h}_{x,c}$  is the representation at the previous layer that gets updated. Note that  $c$  is shorthand notation for  $S^{(c)}$ . Eq. (2) outputs a channel-specific hidden representation  $\mathbf{h}_{x,c}$  for component  $S^{(c)}$  and channel  $x$ . This hidden representation is then passed to the next layer of the SUBGNN architecture.

The order invariance of  $\mathbf{h}_{x,c}$  is a necessary property for layer-to-layer message passing; however, it limits the ability to capture the structure and position of subgraphs [75]. Because of that, we create property-aware output representations,  $\mathbf{z}_{x,c}$ , by producing a matrix of anchor-set messages  $\mathbf{M}_x$ , where each row is an anchor-set message computed by  $\text{MSG}_x$ , and then passing that matrix through a non-linear activation function (Figure 2b and Algorithm 1). In the resulting representation, each dimension of the embedding encodes the structural or positional message from anchor patch  $A$ . For the neighborhood channel, we set  $\mathbf{z}_{N,c} = \mathbf{h}_{N,c}$ . Finally, SUBGNN routes messages for internal and border properties within subchannels for each channel P, N and S, (*i.e.*,  $\{P_I, P_B\}$ ,  $\{N_I, N_B\}$ ,  $\{S_I, S_B\}$ ) and concatenates the final outputs.

Property-aware output representations  $\mathbf{z}_{x,c}$  are transformed into final subgraph representations through order-invariant functions defined at the channel-, layer-, and component-level. Channel-specific representations  $\mathbf{z}_{x,c}$  are first aggregated into a subgraph component representation for each layer, via channel aggregation function  $\text{AGG}_C$ . We then aggregate component representations across all layers via  $\text{AGG}_L$  to produce a final subgraph component representation  $\mathbf{z}_c$  [69]. Finally, the component representations  $\mathbf{z}_c$  for every component  $S^{(c)}$  are aggregated into a final subgraph representation  $\mathbf{z}_S$  via READOUT. A full description of SUBGNN is detailed in Appendix A.

## 4.2 Property-Aware Routing

We enforce property-awareness through the creation of dedicated routing channels for position, neighborhood, and structure. Each channel  $x$  has three key elements: (1) a sampling function  $\phi_x$  to generate anchor patches, (2) an anchor patch encoder  $\psi_x$ , and (3) a similarity function  $\gamma_x$  to weight messages sent between anchor patches and subgraph components.

**(1) Sampling anchor patches.** For each subchannel, we define an anchor patch sampling function  $\phi_x : (G, S^{(c)}) \rightarrow A_x$ . In the position channel, the internal anchor patch sampler  $\phi_{P_I}$  returns patch  $A_{P_I}$  comprised of a single node sampled from subgraph  $S$ . The resulting set of anchor patches  $A_{P_I}$  is shared across all components in  $S$ . This allows representations of  $S$ 's components to be positioned relative to each other. In contrast, the border position anchor patch sampler is designed to position subgraphs relative to the rest of the graph. Accordingly,  $\phi_{P_B}$  samples nodes such that anchor patches  $A_{P_B}$  are shared across all subgraphs. In the neighborhood channel, the internal anchor patch sampler  $\phi_{N_I}$  samples nodes from the subgraph component  $S^{(c)}$ , and the border patch sampler  $\phi_{N_B}$  samples nodes from the  $k$ -hop neighborhood of  $S^{(c)}$ . The structure anchor patch sampler  $\phi_S$  is used for both internal and border structure, and the resulting  $A_{S_I}$  and  $A_{S_B}$  are shared across all  $S$ . In particular,  $\phi_S$  returns a connected component sampled from the graph via triangular random walks, *i.e.*, second-order, biased random walks that extend classical random walks to privilege the traversal of triangles [9] and allow for effective capture of structural properties in graphs [24, 9, 11]. Refer to Appendix A.2 for details.

**(2) Neural encoding of anchor patches.** Each channel  $x$  specifies an anchor patch encoder  $\psi_x : A_x \rightarrow \mathbf{a}_x$  that encodes anchor patch  $A_x$  into a  $d$ -dimensional embedding  $\mathbf{a}_x$ . Note that  $\psi_N$  and  $\psi_P$  simply map to the node embedding of the anchor patch node. In contrast,  $\psi_S$  returns representations of structure anchor patches. To generate representations for the structure anchor patches, we first perform  $w$  fixed-length triangular random walks with parameter  $\beta$  to produce a sequence of traversed nodes  $(u_{\pi_w(1)}, \dots, u_{\pi_w(n)})$  (See Appendix A.2). The resulting sequence of node embeddings is then fed into a bidirectional LSTM, whose hidden states are summed to produce a final representation,  $\mathbf{a}_S$ . To capture the internal structure of the anchor patch, we perform random walks within the anchor patch  $\mathcal{I} = \{u | u \in A_S\}$ . Separately, to capture the border structure of the anchor patch, we perform random walks over the external neighborhood  $\mathcal{E} = \{u | u \notin A_S\}$  and the border nodes  $\mathcal{B} = \{u | u \in \mathcal{I}, v \in \mathcal{E}, e_{uv} \in E\}$ . We limit  $\mathcal{E}$  to external nodes within  $k$  hops of any node in  $A_S$ .

**(3) Estimating similarity of anchor patches.** The similarity function  $\gamma_x : (S^{(c)}, A_x) \rightarrow [0, 1]$  determines the relative weighting of each anchor patch in building the subgraph component representations. In principle,  $\gamma_x$  can be any learned or predefined similarity function. For the position channel, we define  $\gamma_P$  as a function of the shortest path (SP) on the graph between the connected component  $S^{(c)}$  and the anchor patch  $A_P$ ,  $\gamma_P(S^{(c)}, A_P) = 1/(d_{sp}(S^{(c)}, A_P) + 1)$ , where  $d_{sp}$  represents the average SP length. For the neighborhood channel,  $\gamma_N(S^{(c)}, A_N)$  is defined similarly, though note that, due to the sampling schemes, this evaluates to  $\gamma_{N_I} = 1$  in the case of internal neighborhood and  $\gamma_{N_B} \leq k$  in context of the  $k$ -hop border neighborhood sampler. To measure subgraph structure in a permutation-

invariant manner, we compute a canonical input ordering [44], defined by ordered degree sequence, for the component  $S^{(c)}$  and anchor patch  $A_s$ . These are compared using the normalized dynamic time warping (DTW) measure [43]. Specifically, we define  $\gamma_s(S^{(c)}, A_s) = 1/(\text{DTW}(d_{S^{(c)}}, d_{A_s}) + 1)$ , where  $d_{S^{(c)}}$  and  $d_{A_s}$  are the ordered degree sequences for the subgraph component and anchor patch, respectively. The degree for each node  $u \in S^{(c)}$  or  $A_s$  is defined for internal structure as the number of edges from  $u$  to any node  $v \in \mathcal{I}$ , and for border structure as the number of edges from  $u$  to any node  $v \in \mathcal{E}$ .

### 4.3 Implementation and Model Extensions

Below we outline the computational complexity of our SUBGNN implementation and describe its extensions. Details on the training setup and hyperparameters, including a sensitivity analysis of new hyperparameters, are found in Appendix D and E.

**Computational complexity and runtime analysis.** The complexity of SUBGNN scales as the number and size of subgraphs grow. Notably, a fixed number of anchor patches is sampled, which upper bounds the memory and time complexity of the message passing algorithm. Structural anchor patch representations are generated via fixed-length random walks and are only calculated for a small number of anchor patches shared across all subgraphs. We precomputed similarities to speed up hyperparameter optimization, and find that pre-computation results in an 18X training speedup. With pre-computation, training SUB-GNN on the real-world dataset PPI-BP takes 30s per epoch on a single GTX 1080 GPU, of which 25%, 43%, and 32% are spent on neighborhood, position, and structure channels, respectively. Similarity calculation run time could be improved further through approximation methods such as locality sensitive hashing or  $k$ -hop shortest path distances.

**Model extensions.** Our implementation of SUBGNN initializes component embeddings with pre-trained node embeddings, which could alternatively be learned end-to-end. While we specify similarity functions for each channel, we note that  $\gamma_x$  can be replaced with any function measuring the relevance of anchor patches to subgraph components, including learnable similarity functions. Finally, while this paper focuses on subgraph classification, the representation learning modules we present can be trivially extended to any unsupervised, semi-supervised, or other prediction tasks, simply by modifying the loss functions. SUBGNN can also be integrated into other frameworks as a sub-module for end-to-end training.

## 5 Experiments

We first describe our novel datasets, which consist of an underlying base graph and subgraphs with their associated labels. We then describe the baseline approaches and the experimental setup. Finally we present experiments on four synthetic and four real-world datasets for subgraph classification.

**Synthetic datasets.** We construct four datasets with subgraphs of specific graph properties such that binned values of the corresponding metrics act as their labels: DENSITY, CUT RATIO, CORENESS, and COMPONENT. DENSITY challenges the ability of our methods to capture the internal structure of our subgraphs; CUT RATIO, border structure; CORENESS, defined by the average core number of the subgraph, tests border structure and position; and COMPONENT, the number of subgraph components, tests internal and external position. The resulting DENSITY and CUT RATIO datasets have 250 subgraphs of size 20; CORENESS, 221 subgraphs of size 20; and COMPONENT, 250 subgraphs with 15 nodes per component. See Appendix B for more information on the methods used to add subgraphs and basic properties of the datasets.

**PPI-BP dataset.** PPI-BP is a real-world molecular biology dataset. Given a group of genes known to associate with some common biological process, we predict their collective cellular function. The base graph of the PPI-BP dataset is a human protein-protein interaction (PPI) network [85], and subgraphs are collections of proteins in the network involved in the same biological process (e.g., “alcohol biosynthetic process,” “mRNA cleavage,” etc.). Protein subgraphs are labelled according to their cellular function from six categories (e.g. “metabolism”, “development”, etc.).

**HPO-METAB and HPO-NEURO datasets.** HPO-METAB and HPO-NEURO are real-world clinical diagnostic tasks for rare metabolic disorders and neurology, designed to mimic the task of rare disease diagnosis [56, 12, 4]. Given a collection of phenotypes intelligently sampled from a rare disease database, the task is to predict the subcategory of metabolic or neurological disease most

consistent with those phenotypes. The base graph is a knowledge graph containing phenotype and genotype information about rare diseases, and subgraphs consist of collections of phenotypes associated with a rare monogenic disease. HPO-METAB subgraphs are labelled according to the type of metabolic disorder [26, 34, 42], and HPO-NEURO subgraphs are labelled with one or more neurological disorders (multilabel classification) [26, 34].

**EM-USER dataset.** This is a user profiling task. Given the workout history of a user represented by that user’s subgraph, we want to predict characteristics of that user. The base graph is a social fitness network from Endomondo [48], where the nodes represent workouts, and edges exist between workouts completed by multiple users. Each subgraph is represented as an Endomondo subnetwork that make up the user’s workout history, and the labels are characteristics about the user (here, gender). See Appendix B for basic properties of all datasets.

**Alternative baseline approaches.** We consider seven baseline methods that can be applied to training subgraph embeddings. (1) AVG computes the average of the pre-trained node embeddings for nodes in each subgraph. (2) MN-GIN and (3) MN-GAT train meta nodes (also known as virtual nodes) [22, 28, 36] for each subgraph alongside the pre-training of the node embeddings [68, 62]. Both (4) S2V-N and (5) S2V-S compute subgraph embeddings using Sub2Vec [2], each separately preserving the neighborhood and structural properties, respectively. (6) S2V-NS concatenates the subgraph embeddings from S2V-N and S2V-S. Finally, (7) GC is a graph classification GNN (GIN) [19, 68] that aggregates node features from trainable node embeddings to produce subgraph embeddings; for GC, each subgraph is treated as a standalone graph.

**Implementation details.** For each dataset, we first train either GIN [68] or GraphSAINT [77] on link prediction to obtain node and meta node embeddings for the base graph. Sub2Vec subgraph embeddings are trained using the authors’ implementation [2]. For a fair comparison, the feedforward component of all methods, including our own, was implemented as a 3-layer feed forward network with ReLU nonlinear activation and dropout. The feedforward networks were implemented with and without trainable node and subgraph embeddings, and the best results were reported for each. See Appendix D for more training details.

## 6 Results

Table 2: Micro-F1 on synthetic datasets. Standard deviations are provided from runs with 10 random seeds. Here SUBGNN is implemented with GIN node embeddings. See Appendix C for ROC scores. ‘N’ and ‘S’ stand for ‘Neighborhood’ and ‘Structure,’ respectively.

Method	DENSITY	CUT RATIO	CORENESS	COMPONENT
SUBGNN (Ours)	<b>0.919±0.016</b>	<b>0.629±0.039</b>	<b>0.659±0.092</b>	<b>0.958±0.098</b>
Node Averaging	0.429±0.041	0.358±0.055	0.530±0.050	0.516±<0.001
Meta Node (GIN)	0.442±0.052	0.423±0.057	0.611±0.050	0.784±0.046
Meta Node (GAT)	0.690±0.021	0.284±0.052	0.519±0.076	0.935±<0.001
Sub2Vec Neighborhood	0.345±0.066	0.339±0.058	0.381±0.047	0.568±0.039
Sub2Vec Structure	0.339±0.036	0.345±0.121	0.404±0.097	0.510±0.013
Sub2Vec N & S Concat	0.352±0.071	0.303±0.062	0.356±0.050	0.568±0.021
Graph-level GNN	0.803±0.039	0.329±0.073	0.370±0.091	0.500±0.068

**Synthetic datasets.** Results are shown in Tables 2 and 7. We find that our model, SUBGNN, significantly outperforms all baselines by 77.4% and the strongest baseline by 18.4%, on average. Results illustrate relative strengths and weaknesses of baseline models. While the GC method performs quite well on DENSITY (internal structure), as expected, it performs poorly on datasets requiring a notion of position or border connectivity. The MN baselines, in turn, performed best on COMPONENT, presumably because the meta node allows for explicit connection across subgraph components. Sub2Vec, the most directly related prior work, notably did not perform well on any task. This is unsurprising, as Sub2Vec does not explicitly encode position or border structure.

**Channel ablation.** To investigate the ability of our channels to encode their intended properties, we performed an ablation analysis over the channels (Table 4). Results show that performance of individual channels aligns closely with their inductive biases; for example, the structure channel



Table 3: Micro F1 on real-world datasets. Standard deviations are provided from runs with 10 random seeds. We report SUBGNN performance with both GIN and GraphSAINT node embeddings. See Appendix C for ROC scores. ‘N’ and ‘S’ stand for ‘Neighborhood’ and ‘Structure,’ respectively.

Method	PPI-BP	HPO-NEURO	HPO-METAB	EM-USER
SUBGNN (+ GIN)	<b>0.599±0.024</b>	0.632±0.010	<b>0.537±0.023</b>	0.814±0.046
SUBGNN (+ GraphSAINT)	0.583±0.017	<b>0.644±0.019</b>	0.428±0.035	0.816±0.040
Node Averaging	0.297±0.027	0.490±0.059	0.443±0.063	0.808±0.138
Meta Node (GIN)	0.306±0.025	0.233±0.086	0.151±0.073	0.480±0.089
Meta Node (GAT)	0.307±0.021	0.259±0.063	0.138±0.034	0.471±0.048
Sub2Vec Neighborhood	0.306±0.009	0.211±0.068	0.132±0.047	0.520±0.090
Sub2Vec Structure	0.306±0.021	0.223±0.065	0.124±0.025	<b>0.859±0.014</b>
Sub2Vec N & S Concat	0.309±0.023	0.206±0.073	0.114±0.021	0.522±0.043
Graph-level GNN	0.398±0.058	0.535±0.032	0.452±0.025	0.561±0.059

performs best on CUT RATIO (a border structure task) and DENSITY (an internal structure task), and the position channel performs best on COMPONENT (an internal position task). The CORENESS task primarily measures internal structure but also incorporates notions of border position; we find that the structure channel and combined channels perform best on this task.

Table 4: Channel ablation analyses (Micro F1). Channels that encode properties relevant to each dataset have a ✓ and best performing channels are in **bold**. We see in each case that the channels designed to encode relevant properties yield the best performance on each dataset. This suggests that the SUBGNN channels successfully encode their desired properties.

SUBGNN Channel	DENSITY	CUT RATIO	CORENESS	COMPONENT
Position (P)	0.758±0.046	0.516±0.083	0.581±0.044 ✓	<b>0.958±0.098</b> ✓
Neighborhood (N)	0.777±0.057	0.313±0.087	0.485±0.075	0.823±0.089
Structure (S)	<b>0.919±0.016</b> ✓	<b>0.629±0.039</b> ✓	<b>0.663±0.058</b> ✓	0.600±0.170
All (P+N+S)	0.894±0.025	0.458±0.101	0.659±0.092	0.726±0.120

**Real-world datasets.** Results are shown in Tables 3 and 8. We find that our model performs strongly on real-world datasets, outperforming baselines by 125.2% on average and performs 21.2% better than the strongest baseline. We experiment with both GIN and GraphSAINT node embeddings and find that each yields performance gains on different datasets. SUBGNN performed especially well relative to baselines on the HPO-NEURO and HPO-METAB tasks. These tasks are uniquely challenging because they require distinguishing subcategories of similar diseases (a challenge for averaging-based methods), exhibit class distributional shift between train and test, and have been designed to require inductive inference to nearby phenotypes using edges in the graph. Strong performance of SUBGNN on these tasks thus suggests the ability of our model to leverage its relational inductive biases for more robust generalization. Further results studying the generalizability of SUBGNN are in Appendix C. One baseline, s2v-s, achieved a higher micro F1 score, but lower AUC compared to SUBGNN on the EM-USER dataset. Finally, our model outperformed all baselines on the PPI-BP task, which like the HPO tasks operates over non-trivial biological subgraphs. Taken together, all of our new datasets are non-trivial and present unique challenges that highlight the relative strengths and weakness of existing methods in the field.

## 7 Conclusion

We present SUBGNN, a novel method for subgraph representation learning and classification, along with a framework outlining the key representational challenges facing the field. SUBGNN performs subgraph level message passing with property-aware channels. We present eight new datasets (4 synthetic, 4 real-world) representing a diverse collection of tasks that we hope will stimulate new subgraph representation learning research. SUBGNN outperforms baselines by an average of 77.4% on synthetic datasets and 125.2% on real-world datasets.

## Broader Impact

**A variety of impactful application areas.** The ability of SUBGNN to learn powerful subgraph representations creates fundamentally new opportunities for applications beyond the reach of node-, edge-, and graph-level tasks. Such applications require us to be able to reason about subgraphs and predict properties of subgraphs by leveraging the fact that subgraphs reside within a large, underlying graph. For example, this work was directly motivated by the challenge of rare disease diagnosis, which motivated the generation of two new datasets that we are releasing specifically to foster methods that will eventually prove useful on subgraph predict tasks (*e.g.*, patient subgraphs residing within a large biomedical knowledge graph). Likewise, drug development represents another broad potential area of research that is closely connected with the field of graph neural networks. Hence, we also developed a new bioinformatics dataset. In addition, there are many other potentially positive applications for this class of method, including the prediction of toxic behavior on social media.

**The need for thoughtful use of SUBGNN framework.** We also recognize that Subgraph Neural Networks have potential to be used for harmful applications. For example, the potential benefit of predicting toxic communities on social media is inextricably tied with the capacity to leverage these same networks for malicious political and social purposes. Another broad class of harms that could involve subgraph classification include those harms that emerge from high-resolution user profiling. As with any data-driven methods, there is also an opportunity for bias to exist at all stages of the model development process. In the case of biomedical data science, for example, biases can exist within the data itself, and disparities can exist both in their efficacy as well as their deployment reach.

**Real-world subgraph datasets.** The release of our monogenic disease and bioinformatics datasets is, in large part, motivated by our desire to help steer the community towards beneficial rather than malicious applications of these tools. Ultimately, given the relative immaturity of this field among major areas of computer science, vigilance is required on the part of researchers (and other relevant experts) to ensure that we as a community pursue the best possible use of our tools.

## Acknowledgments and Disclosure of Funding

S.G.F. was supported by training grant T32GM007753 from the National Institute of General Medical Science, NIH. M.M.L. was supported by T32HG002295 from the National Human Genome Research Institute, NIH. M.Z. is supported, in part, by NSF grant nos. IIS-2030459 and IIS-2033384, and by the Harvard Data Science Initiative. The content is solely the responsibility of the authors.

## References

- [1] Sami Abu-El-Haija et al. “Mixhop: Higher-order graph convolution architectures via sparsified neighborhood mixing”. In: *ICML* (2019).
- [2] Bijaya Adhikari et al. “Sub2vec: Feature learning for subgraphs”. In: *PAKDD*. Springer. 2018.
- [3] Michael Ashburner et al. “Gene ontology: tool for the unification of biology”. In: *Nature Genetics* 25.1 (2000).
- [4] Christopher P Austin and Hugh JS Dawkins. “Next decade’s goals for rare diseases”. In: *Nature* 548.7666 (2017), pp. 158–158.
- [5] Jiyang Bai, Yuxiang Ren, and Jiawei Zhang. “Ripple Walk Training: A Subgraph-based training framework for Large and Deep Graph Neural Network”. In: *arXiv:2002.07206* (2020).
- [6] Yunsheng Bai et al. “Unsupervised inductive graph-level representation learning via graph-graph proximity”. In: *IJCAI*. 2019.
- [7] Peter W Battaglia et al. “Relational inductive biases, deep learning, and graph networks”. In: *arXiv:1806.01261* (2018).
- [8] Austin R Benson, David F Gleich, and Jure Leskovec. “Higher-order organization of complex networks”. In: *Science* 353.6295 (2016).
- [9] Paolo Boldi and Marco Rosa. “Arc-community detection via triangular random walks”. In: *Eighth Latin American Web Congress*. 2012.
- [10] Antoine Bordes, Sumit Chopra, and Jason Weston. “Question answering with subgraph embeddings”. In: (2014).

- [11] JN Boyd and PN Raychowdhury. “Discrete Dirichlet problems, convex coordinates, and a random walk on a triangle”. In: *The College Mathematics Journal* 20.5 (1989).
- [12] Conor A Bradley. “A statistical framework for rare disease diagnosis”. In: *Nature Reviews Genetics* 21.1 (2020), pp. 2–3.
- [13] Wei-Lin Chiang et al. “Cluster-GCN: An efficient algorithm for training deep and large graph convolutional networks”. In: *KDD*. 2019.
- [14] Gene Ontology Consortium. “The gene ontology resource: 20 years and still GOing strong”. In: *Nucleic Acids Research* 47.D1 (2019).
- [15] Fabrizio Costa and Kurt De Grave. “Fast neighborhood subgraph pairwise distance kernel”. In: *ICML*. 2010.
- [16] Claire Donnat et al. “Learning structural node embeddings via diffusion wavelets”. In: *KDD*. 2018.
- [17] WA Falcon. “PyTorch Lightning”. In: *GitHub*. Note: <https://github.com/williamFalcon/pytorch-lightning> Cited by 3 (2019).
- [18] Fuli Feng et al. “Learning on partial-order hypergraphs”. In: *WWW*. 2018.
- [19] Matthias Fey and Jan E. Lenssen. “Fast Graph Representation Learning with PyTorch Geometric”. In: *ICLR Workshop on Representation Learning on Graphs and Manifolds*. 2019.
- [20] Pablo Gainza et al. “Deciphering interaction fingerprints from protein molecular surfaces using geometric deep learning”. In: *Nature Methods* 17.2 (2020).
- [21] Zheng Gao et al. “edge2vec: Representation learning using edge semantics for biomedical knowledge discovery”. In: *BMC Bioinformatics* 20.1 (2019).
- [22] Justin Gilmer et al. “Neural message passing for quantum chemistry”. In: *ICML*. 2017.
- [23] Palash Goyal and Emilio Ferrara. “Graph embedding techniques, applications, and performance: A survey”. In: *Knowledge-Based Systems* 151 (2018), pp. 78–94.
- [24] Keming Gu and Matthew NO Sadiku. “A triangular mesh random walk for Dirichlet problems”. In: *Journal of the Franklin Institute* 332.5 (1995).
- [25] Will Hamilton, Zhitao Ying, and Jure Leskovec. “Inductive representation learning on large graphs”. In: *NIPS*. 2017.
- [26] Taila Hartley et al. “New Diagnostic Approaches for Undiagnosed Rare Genetic Diseases”. In: *Annual Review of Genomics and Human Genetics* 21 (2020).
- [27] Weihua Hu et al. “Strategies for pre-training graph neural networks”. In: *ICLR*. 2020.
- [28] Katsuhiko Ishiguro, Shin-ichi Maeda, and Masanori Koyama. “Graph warp module: an auxiliary module for boosting the power of graph neural networks”. In: *arXiv:1902.01020* (2019).
- [29] Jianwen Jiang et al. “Dynamic hypergraph neural networks”. In: *IJCAI*. 2019.
- [30] Di Jin et al. “Latent network summarization: Bridging network embedding and summarization”. In: *KDD*. 2019.
- [31] Taisong Jin et al. “Hypergraph induced convolutional manifold networks”. In: *IJCAI*. 2019.
- [32] Pan-Jun Kim and Nathan D Price. “Genetic co-occurrence network across sequenced microbes”. In: *PLoS Computational Biology* 7.12 (2011).
- [33] Thomas N Kipf and Max Welling. “Semi-supervised classification with graph convolutional networks”. In: *ICLR* (2017).
- [34] Sebastian Kohler et al. “Expansion of the Human Phenotype Ontology (HPO) knowledge base and resources”. In: *Nucleic Acids Research* (2019).
- [35] Yuko Kuroki et al. “Online dense subgraph discovery via blurred-graph feedback”. In: *ICML* (2020).
- [36] Junying Li, Deng Cai, and Xiaofei He. “Learning graph-level representation for drug discovery”. In: *arXiv:1709.03741* (2017).
- [37] Qi Li et al. “Graph representation learning with encoding edges”. In: *Neurocomputing* 361 (2019).
- [38] Donna Maglott et al. “Entrez Gene: gene-centered information at NCBI”. In: *Nucleic Acids Research* 33.suppl\_1 (2005).
- [39] Sylvie Maiella et al. “Orphanet and its consortium: where to find expert-validated information on rare diseases”. In: *Revue Neurologique* 169 (2013).

- [40] Changping Meng et al. “HATS: A Hierarchical Sequence-Attention Framework for Inductive Set-of-Sets Embeddings”. In: *KDD*. 2019.
- [41] Changping Meng et al. “Subgraph pattern neural networks for high-order graph evolution prediction”. In: *AAAI*. 2018.
- [42] Dylan Mordaunt, David Cox, and Maria Fuller. “Metabolomics to Improve the Diagnostic Efficiency of Inborn Errors of Metabolism”. In: *International Journal of Molecular Sciences* 21.4 (2020).
- [43] Abdullah Mueen and Eamonn Keogh. “Extracting optimal performance from dynamic time warping”. In: *Proceedings of the 22nd ACM SIGKDD International Conference on Knowledge Discovery and Data Mining*. 2016, pp. 2129–2130.
- [44] Ryan L Murphy et al. “Janosy pooling: Learning deep permutation-invariant functions for variable-size inputs”. In: *ICLR* (2019).
- [45] Ryan L Murphy et al. “Relational pooling for graph representations”. In: *ICML* (2019).
- [46] Mark EJ Newman. “Detecting community structure in networks”. In: *The European Physical Journal B* 38.2 (2004).
- [47] Mark EJ Newman and Aaron Clauset. “Structure and inference in annotated networks”. In: *Nature Communications* 7.1 (2016).
- [48] Jianmo Ni, Larry Muhlstein, and Julian McAuley. “Modeling Heart Rate and Activity Data for Personalized Fitness Recommendation”. In: *WWW*. 2019.
- [49] Mathias Niepert, Mohamed Ahmed, and Konstantin Kutzkov. “Learning Convolutional Neural Networks for Graphs”. In: *ICML*. 2016.
- [50] Janet Piñero et al. “DisGeNET: a comprehensive platform integrating information on human disease-associated genes and variants”. In: *Nucleic Acids Research* (2016).
- [51] Bastian Rieck et al. “Clique community persistence: A topological visual analysis approach for complex networks”. In: *IEEE Transactions on Visualization and Computer Graphics* 24.1 (2017).
- [52] Peter N Robinson et al. “The Human Phenotype Ontology: a tool for annotating and analyzing human hereditary disease”. In: *The American Journal of Human Genetics* 83.5 (2008).
- [53] Ahmet Erdem Sariyuce et al. “Finding the hierarchy of dense subgraphs using nucleus decompositions”. In: *WWW*. 2015.
- [54] Sai Nageswar Satchidanand, Harini Ananthapadmanaban, and Balaraman Ravindran. “Extended discriminative random walk: a hypergraph approach to multi-view multi-relational transductive learning”. In: *IJCAI*. 2015.
- [55] Stephen B Seidman. “Network structure and minimum degree”. In: *Social Networks* 5.3 (1983).
- [56] Kimberly Splinter et al. “Effect of genetic diagnosis on patients with previously undiagnosed disease”. In: *New England Journal of Medicine* 379.22 (2018), pp. 2131–2139.
- [57] Aravind Subramanian et al. “Gene set enrichment analysis: a knowledge-based approach for interpreting genome-wide expression profiles”. In: *Proceedings of the National Academy of Sciences* 102.43 (2005).
- [58] Fan-Yun Sun et al. “vGraph: A Generative Model for Joint Community Detection and Node Representation Learning”. In: *NeurIPS*. 2019.
- [59] Komal K Teru, Etienne Denis, and William L Hamilton. “Inductive Relation Prediction by Subgraph Reasoning”. In: *ICML*. 2020.
- [60] Ruo-Chun Tzeng and Shan-Hung Wu. “Distributed, Egocentric Representations of Graphs for Detecting Critical Structures”. In: *ICML*. 2019.
- [61] Petar Veličković et al. “Deep Graph Infomax”. In: *ICLR*. 2019. URL: <https://openreview.net/forum?id=rklz9iAcKQ>.
- [62] Petar Veličković et al. “Graph attention networks”. In: *ICLR*. 2018.
- [63] Pengyang Wang et al. “Adversarial Substructured Representation Learning for Mobile User Profiling”. In: *KDD*. 2019.
- [64] Chris Wendler, Markus Püschel, and Dan Alistarh. “Powerset convolutional neural networks”. In: *NIPS*. 2019.
- [65] Zonghan Wu et al. “A comprehensive survey on graph neural networks”. In: *arXiv:1901.00596* (2019).

- [66] Zonghan Wu et al. “A comprehensive survey on graph neural networks”. In: *IEEE Transactions on Neural Networks and Learning Systems* (2020).
- [67] Jierui Xie, Stephen Kelley, and Boleslaw K Szymanski. “Overlapping community detection in networks: The state-of-the-art and comparative study”. In: *ACM CSUR* 45.4 (2013).
- [68] Keyulu Xu et al. “How Powerful are Graph Neural Networks?” In: *ICLR*. 2019.
- [69] Keyulu Xu et al. “Representation learning on graphs with jumping knowledge networks”. In: *ICML*. 2018.
- [70] Naganand Yadati et al. “HyperGCN: A New Method For Training Graph Convolutional Networks on Hypergraphs”. In: *NeurIPS*. 2019.
- [71] Jaewon Yang and Jure Leskovec. “Defining and evaluating network communities based on ground-truth”. In: *Knowledge and Information Systems* 42.1 (2015).
- [72] Zichao Yang et al. “Hierarchical attention networks for document classification”. In: *Proceedings of the 2016 Conference of the North American Chapter of the Association for Computational Linguistics: Human Language Technologies*. 2016.
- [73] Zhitao Ying et al. “GNNExplainer: Generating explanations for graph neural networks”. In: *NeurIPS*. 2019.
- [74] Tomoki Yoshida, Ichiro Takeuchi, and Masayuki Karasuyama. “Learning interpretable metric between graphs: Convex formulation and computation with graph mining”. In: *KDD*. 2019.
- [75] Jiaxuan You, Rex Ying, and Jure Leskovec. “Position-aware graph neural networks”. In: *ICML*. 2019.
- [76] Manzil Zaheer et al. “Deep sets”. In: *NeurIPS*. 2017.
- [77] Hanqing Zeng et al. “GraphSAINT: Graph Sampling Based Inductive Learning Method”. In: *ICLR*. 2020.
- [78] Muhan Zhang and Yixin Chen. “Link prediction based on graph neural networks”. In: *NeurIPS*. 2018.
- [79] Muhan Zhang et al. “Beyond link prediction: Predicting hyperlinks in adjacency space”. In: *AAAI*. 2018.
- [80] Ruochi Zhang, Yuesong Zou, and Jian Ma. “Hyper-SAGNN: a self-attention based graph neural network for hypergraphs”. In: *ICLR*. 2020.
- [81] Ziwei Zhang, Peng Cui, and Wenwu Zhu. “Deep learning on graphs: A survey”. In: *IEEE Transactions on Knowledge and Data Engineering* (2020).
- [82] Dengyong Zhou, Jiayuan Huang, and Bernhard Schölkopf. “Learning with hypergraphs: Clustering, classification, and embedding”. In: *NIPS*. 2007.
- [83] Jie Zhou et al. “Graph neural networks: A review of methods and applications”. In: *arXiv:1812.08434* (2018).
- [84] Marinka Zitnik, Monica Agrawal, and Jure Leskovec. “Modeling polypharmacy side effects with graph convolutional networks”. In: *Bioinformatics* 34.13 (2018).
- [85] Marinka Zitnik et al. *BioSNAP Datasets: Stanford Biomedical Network Dataset Collection*. <http://snap.stanford.edu/biodata>. Aug. 2018.

## Appendix A Further Details on SUBGNN

In this section, we outline additional details and design decisions for the implementation of SUBGNN. In Section A.1, we provide an algorithmic overview of our method, and in Section A.2, we provide further motivation and details on triangular random walks and the structural anchor patch embedder algorithm.

### A.1 Message Passing Algorithm

For brevity, Algorithm 1 summarizes the forward pass of SUBGNN for a single subgraph  $S$ . While the algorithm demonstrates how to embed subgraph  $S$ , we want to emphasize that SUBGNN learns representations for every subgraph  $S \in \{S_1, S_2, \dots, S_n\}$ . In practice, we extend Algorithm 1 to multiple subgraphs using mini-batching. Note that any aggregation function that operates over an unordered set of vectors can be used for  $\text{AGG}_M$ ,  $\text{AGG}_C$ ,  $\text{AGG}_L$ , and/or  $\text{READOUT}$ . Our implementation leverages the sum operator for  $\text{AGG}_M$  and  $\text{READOUT}$  and the concat operator for  $\text{AGG}_C$  and  $\text{AGG}_L$ . We empirically found that applying attention [72] over the individual subgraph component representations did not yield any performance gains over summation for  $\text{READOUT}$ .

---

**Algorithm 1:** SUBGRAPH NEURAL NETWORK. Channels N, S, and P correspond to neighborhood, structure, and position. Subchannels I and B correspond to internal and border subgraph topology.

---

**Input:** Graph  $G = (V, E)$ ; Node representations  $\{\mathbf{x}_u | u \in V\}$ ; Subgraph  $S$  consisting of connected components  $S^{(c)}$  for  $c = 1, \dots, n_c$ ; Anchor patch sampler  $\phi_x$ , anchor patch encoder  $\psi_x$ , and anchor patch similarity function  $\gamma_x$  for each channel  $x$ ; Nonlinear activation function  $\sigma$

**Output:** Subgraph representation  $\mathbf{h}_S$  for subgraph  $S$

**Model Parameters:** Layer-wise, channel-specific learnable weight matrices  $\mathbf{W}_x$  and  $\mathbf{Q}_x$

```

 $\mathbf{z}_c^{(0)} = \sum_{u \in S^{(c)}} \mathbf{x}_u$ 
 $\mathbf{h}_{x,c}^{(0)} = \mathbf{z}_c^{(0)}$  for channel  $x \in \{N, S, P\}$  // Channel-independent initialization
for layer  $l = 1, \dots, L$  do
   $A_x^{(i)} = \phi_x(G)$  for  $i = 1, \dots, n_A$  and channel  $x \in \{S_I, S_B, P_B\}$  // See Section 4.2
   $A_x^{(i)} = \phi_x(G, S)$  for  $i = 1, \dots, n_A$  and channel  $x \in \{P_I\}$ 
  for connected component  $c = 1, \dots, n_c$  do
     $A_x^{(i)} = \phi_x(G, S^{(c)})$  for  $i = 1, \dots, n_A$  and channel  $x \in \{N_I, N_B\}$ 
    for channel  $x \in \{\{P_I, P_B\}, \{N_I, N_B\}, \{S_I, S_B\}\}$  do
      for anchor patch  $i = 1, \dots, n_A$  do
         $\mathbf{a}_x^{(i)} = \psi_x(A_x^{(i)})$  // E.g., Algorithm 2
         $\mathbf{m}_{x,c,i}^{(l)} = \text{MSG}_x^{A_x^{(i)} \rightarrow S^{(c)}}$  // (Eq.1)
         $\mathbf{M}_{x,c}^{(l)}[i] = \mathbf{m}_{x,c,i}^{(l)}$  if  $x \in \{S_*, P_*\}$ 
      end
       $\mathbf{z}_{x,c}^{(l)} = \sigma(\mathbf{Q}_x^{(l)} \cdot \mathbf{M}_{x,c}^{(l)})$  if  $x \in \{S_*, P_*\}$  // Property-aware output rep.
       $\mathbf{g}_{x,c}^{(l)} = \text{AGG}_M(\{\mathbf{m}_{x,c,1}^{(l)}, \dots, \mathbf{m}_{x,c,n_A}^{(l)}\})$  // Aggregate messages (Eq.2)
       $\mathbf{h}_{x,c}^{(l)} = \sigma(\mathbf{W}_x^{(l)} \cdot [\mathbf{g}_{x,c}^{(l)}; \mathbf{h}_{x,c}^{(l-1)}])$  // Order-invariant rep. (Eq.2)
    end
     $\mathbf{z}_c^{(l)} = \text{AGG}_C(\mathbf{h}_{N,c}^{(l)}, \mathbf{z}_{S,c}^{(l)}, \mathbf{z}_{P,c}^{(l)})$  // Aggregate channels
  end
end
 $\mathbf{z}_c \leftarrow \text{AGG}_L(\{\mathbf{z}_c^{(0)}, \dots, \mathbf{z}_c^{(L)}\})$  // Aggregate layers
 $\mathbf{h}_S = \text{READOUT}(\{\mathbf{z}_1, \dots, \mathbf{z}_{n_c}\})$  // Aggregate subgraph components

```

---

## A.2 Triangular Random Walks

In Section 4.2, we leverage triangular random walks [9] to (1) sample structure anchor patches via  $\phi_s$  and (2) embed the structure anchor patches via  $\psi_s$ . Refer to Algorithm 2 for a summary of the structure anchor patch embedder.

Triangular random walks are parameterized by  $\beta \in [0, 1]$  and yield a sequence of nodes  $X_0, X_1, \dots, X_n$ . The parameter  $\beta$  determines whether triangles or non-triangles will be privileged during sampling. A node  $z$  is said to be a triangular successor to nodes  $x$  and  $y$  if  $x, y, z$  would form a triangle. The triangular random walk samples triangular successors with probability  $\beta$  and non-triangular successors with probability  $1 - \beta$ . When performing an internal random walk, we initialize  $P[X_0 = x] = 1/|\mathcal{I}|$  and  $P[X_1 = y|X_0 = x] = 1/d_I(x)$ , where  $d_I(x)$  is number of edges from  $x$  to other nodes in  $\mathcal{I}$ . Similarly, we initialize a border random walk with  $P[X_0 = x] = 1/|\mathcal{B}|$  and  $P[X_1 = y|X_0 = x] = 1/d_E(x)$  where  $d_E(x)$  is number of edges from  $x$  to nodes in  $\mathcal{E}$ .

We then define the transition probability for any subsequent step of the random walk as follows: given current node  $y$  and preceding node  $x$ , the probability of transition to node  $z$  is defined as  $P[X_{t+1} = z|X_t = y, X_{t-1} = x] = [\beta(1/|T|)\mathbb{1}_{X_{t+1} \in T} + (1 - \beta)(1/|U|)\mathbb{1}_{X_{t+1} \in U}]$  where  $T$  is the set of triangular successors of nodes  $x$  and  $y$  and  $U$  is the set of non-triangular successors. More precisely,  $T(X_t, X_{t-1}) = N(X_t) \cap N(X_{t-1})$  and  $U(X_t, X_{t-1}) = N(X_t) \setminus N(X_{t-1})$ .

---

### Algorithm 2: STRUCTURE ANCHOR PATCH EMBEDDER.

---

**Input:** Graph  $G$ ; Anchor patch  $A$ ; Node representations  $\{\mathbf{x}_u|u \in A\}$ ; Triangle random walk (TRIANGLE\_RW) parameter  $\beta$ ; Number of walks  $n$ ; Length of walks  $k$

**Output:** Representation  $\mathbf{a}$  for anchor patch  $A$

**for**  $i = 1, \dots, n$  **do**

$(u_{\pi(1)}, \dots, u_{\pi(k)}) = \text{TRIANGLE\_RW}(G, A, \beta)$   
 $\mathbf{h}_i = \text{BI-LSTM}(\{\mathbf{x}_{\pi(1)}, \dots, \mathbf{x}_{\pi(k)}\})$  where  $\mathbf{x}_{\pi(j)}$  is representation for node  $u_{\pi(j)}$

**end**

$\mathbf{a} = \sum_{i=1, \dots, n} \mathbf{h}_i$

---

## Appendix B Further Details on Datasets

We proceed by describing the construction and processing of synthetic as well as real-world datasets. Note that we provide all datasets in our SUBGNN code release.

### B.1 Synthetic Datasets for Subgraph Classification

**Generating base graphs.** For DENSITY, CUT RATIO, and COMPONENT, we start with a base Barabási-Albert graph, where the number of preferentially attached edges,  $m$ , is 5 for DENSITY and CUT RATIO and  $m = 1$  for DIAMETER and COMPONENT. In CORENESS, the base graph is a duplication-divergence graph where the probability of retaining the edge of the replicated node is 0.7. Refer to Table 5 for properties of the base graphs.

**Generating subgraphs.** We introduce three methods for generating subgraphs: (1) the PLANT method, which searches for  $n > 1$  common nodes and  $e \geq 1$  shared edges between the base graph and the new subgraph, and plants the subgraph on the base graph via the union of the node and edge sets; (2) the STAPLE method, which adds an edge between a randomly sampled node in the base graph and a node in the new subgraph; and (3) the BFS method, which creates subgraphs in the base graph by performing breadth first search with a specified max depth  $d$  from randomly selected start nodes. Figure 3 describes the PLANT and STAPLE approaches in more detail.

We construct subgraphs with various desired graph properties: density, cut ratio,  $k$ -coreness, and number of components [71, 55]. Density is defined as  $D = (2 \cdot |E|)/(|V| \cdot |V - 1|)$  for our undirected graphs. We define cut ratio as the proportion of edges shared between the subgraph  $S$  and the rest of the graph  $G$ , specifically  $\text{CR}(S) = |\mathcal{B}_S|/(|S||G \setminus S|)$ , where  $\mathcal{B}_S = \{(u, v) \in E|u \in S, v \in G \setminus S\}$ . The  $k$ -core of a graph is the maximum subgraph with a minimum degree of at least  $k$ . A connected component is defined as a set of nodes in a subgraph such that each pair of nodes is connected by a path.

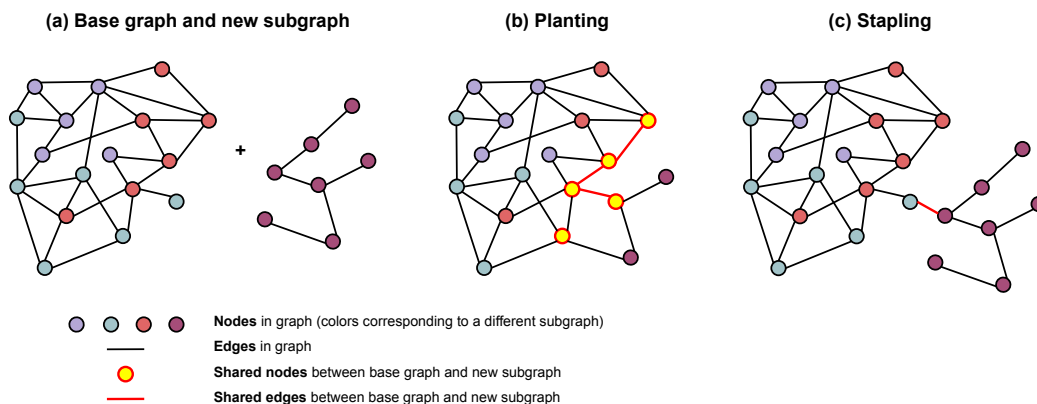


Figure 3: Procedures for generating synthetic graphs. (a) Base graph and new subgraph to be added. (b) New synthetic graph with a “planted” subgraph. (c) New synthetic graph with a “stapled” subgraph. The base graph (a) has 3 subgraphs, and the new graphs (b)-(c) each have 4 subgraphs, indicated by the colors red, light blue, light purple, and dark purple. The yellow nodes and bright red edges are those shared between the base graph and the new subgraph.

**Subgraph classification tasks.** For each subgraph classification task, we generate subgraphs that vary along a specific network property (e.g. density, cut ratio). Labels are then generated by binning the network property values into two or three quantiles: (1) DENSITY has 250 subgraphs that are constructed via BFS with  $d = 3$  to have low, medium, or high density. (2) CUT RATIO has 250 subgraphs constructed by PLANTING complete graphs onto the base graph such that the subgraphs have low, medium, or high cut ratio. (3) CORENESS has 221 subgraphs that are created using the duplication-divergence model and constructed via PLANTING onto the base graph. These subgraphs’ labels (e.g., low, medium, or high coreness bins) are assigned by calculating the average  $k$ -coreness of all nodes in the subgraph. Finally, (4) COMPONENT contains 250 Barabási-Albert subgraphs that are STAPLED onto the base graph, and the associated label is the number of connected components in the subgraph (single or multiple components). Subgraphs for synthetic datasets are split into train, validation, and test sets via a 50/25/25 split. See Table 6 for properties of subgraphs in the datasets.

## B.2 Novel, Real-World Datasets for Subgraph Classification

**PPI-BP dataset.** The base graph of the PPI-BP dataset is a human protein-protein interaction (PPI) network [85], which contains 17,080 nodes and 630,226 edges. Nodes represent human proteins specified by their Entrez IDs [38], and edges exist between nodes if there is physical interaction between the proteins. Subgraphs are collections of proteins in the PPI network involved in the same biological process (e.g., “alcohol biosynthetic process,” “mRNA cleavage,” etc.). These subgraphs were obtained from the Gene Ontology (GO) gene sets from the Molecular Signatures Database (MSigDB) [57]. PPI-BP subgraphs labels are obtained from the “GO Slim” resource in the GO Biological Process Ontology [14, 3], which groups narrow processes into broader categories: metabolism, development, signal transduction, stress/death, cell organization, and transport. Gene sets are limited to those containing at least five genes, and we exclude any gene sets that comprised 70% or more of the genes in any other gene set. Subgraphs are split 80/10/10 at random into training, validation, and test sets. There are on average 10.2 nodes per subgraph and 265.2 subgraphs across the 6 labels [57].

**HPO-NEURO dataset.** The base graph is a knowledge graph containing phenotype and genotype information about rare diseases. Nodes are phenotypes (symptoms), and edges exist between phenotypes if (1) they are caused by a mutation in a shared gene according to DisGeNET [50], HPO-A [34], or Orphanet [39] or (2) an edge exists between the phenotypes according to the Human Phenotype Ontology (HPO) [52]. Each subgraph consists of a set of phenotypes associated with a rare monogenic disease. The subgraphs contain noisy phenotypes unrelated to the disease, distractor phenotypes related to incorrect but similar diseases, and less specific phenotypes generated by walking up the HPO hierarchy (e.g., from “arachnodactyly” to “abnormality of the fingers”). Together, these simulate the imperfect diagnosis process and make the diagnosis task more realistic. Subgraph



Table 5: Properties of **base graphs** in synthetic and real-world datasets.

Dataset	# Nodes	# Edges	Density	# Subgraphs	# Labels
DENSITY	5,000	29,521	0.0024	250	3
CUT RATIO	5,000	83,969	0.0067	250	3
CORENESS	5,000	118,785	0.0095	221	3
COMPONENT	19,555	43,701	0.0002	250	2
PPI-BP	17,080	316,951	0.0022	1,591	6
HPO-METAB	14,587	3,238,174	0.0304	2,400	6
HPO-NEURO	14,587	3,238,174	0.0304	4,000	10
EM-USER	57,333	4,573,417	0.0028	324	2

Table 6: Properties of **subgraphs** in synthetic and real-world datasets.

Dataset	Average # nodes	Average density	Average cut ratio	Average # components
DENSITY	20.0±0.0	0.232±0.146	0.0010±0.0062	3.8±3.7
CUT RATIO	20.0±0.0	0.945±0.028	0.0072±0.0011	1.0±0.0
CORENESS	20.0±0.0	0.219±0.062	0.0082±0.0081	1.0±0.0
COMPONENT	74.2±52.8	0.150±0.161	$5.1 \times 10^{-6} \pm 3.4 \times 10^{-6}$	4.9±3.5
PPI-BP	10.2±10.5	0.216±0.188	0.0036±0.0032	7.0±5.5
HPO-METAB	14.4±6.2	0.757±0.149	0.1844±0.0396	1.6±0.7
HPO-NEURO	14.8±6.5	0.767±0.141	0.1834±0.0386	1.5±0.7
EM-USER	155.4±100.2	0.010±0.006	0.0053±0.0006	52.1±15.3

labels are the diagnosis categories. This is a multi-label dataset consisting of 10 neurological disease categories: neurodegenerative, epilepsy, ataxia, genetic dementia, central nervous system malformation, intellectual, neurometabolic, movement, peripheral neuropathy, and neuromuscular disease. Subgraphs are split by disease into train, validation, and test sets via an 80/10/10 split.

**HPO-METAB dataset.** This is a clinical diagnostic task for rare metabolic disorders, defined similarly to HPO-NEURO, but for a different collection of diseases and disease categories. The base graph is identical to the base graph in HPO-NEURO, and the subgraphs consist of a set of phenotypes associated with a rare monogenic metabolic disease. The HPO-METAB dataset contains 6 labels corresponding to types of metabolic disease: lysosomal, energy, amino acid, carbohydrate, lipid, and glycosylation. Subgraphs are split by disease into train, validation, and test sets via an 80/10/10 split.

**EM-USER dataset.** The Endomondo base graph is a co-occurrence network: nodes represent workouts, and edges exist between workouts completed by multiple users. As such, the graph contains cliques (*i.e.*, small fully connected networks) of highly popular combinations of workouts. We identify co-occurrence cliques and use random network sampling to break up cliques in the base graph [32, 51]. Examples are split 75/15/15 by workout into train, validation, and test sets.

See Table 5 and 6 for further properties of all datasets.

## Appendix C Details on Empirical Evaluation

Baseline models and SUBGNN were evaluated using Micro F1 and AUROC. Both metrics were implemented using Scikit-learn (Version 0.20.2). AUROC scores for synthetic datasets are in Table 7, and results for real-world datasets are in Table 8. AUROC scores for the SUBGNN channel ablation analysis are in Table 9.

**Generalizability analysis.** Generalizability in subgraph representation learning is an interesting area of future research, in part because in this context it could be defined in several competing ways. For example, one aspect of generalizability in subgraph prediction is the ability to make predictions about subgraphs that contain *nodes* that were never seen during training. To probe this aspect of SUBGNN, we measure the test performance of the model as a function of the overlap in nodes between train and

Table 7: AUROC performance on synthetic datasets. Standard deviations are provided from runs with 10 random seeds. ‘N’ and ‘S’ stand for ‘Neighborhood’ and ‘Structure,’ respectively.

Method	Datasets			
	DENSITY	CUT RATIO	CORENESS	COMPONENT
SUBGNN (Ours)	<b>0.971±0.007</b>	<b>0.836±0.021</b>	<b>0.824±0.044</b>	<b>0.997±0.009</b>
Node Averaging	0.619±0.026	0.542±0.069	0.700±0.028	0.623±0.199
Meta Node (GIN)	0.602±0.039	0.602±0.023	0.670±0.047	0.873±0.026
Meta Node (GAT)	0.809±0.024	0.531±0.089	0.682±0.068	0.884±0.014
Sub2Vec Neighborhood	0.580±0.028	0.533±0.046	0.592±0.037	0.629±0.035
Sub2Vec Structure	0.553±0.026	0.504±0.093	0.539±0.084	0.539±0.104
Sub2Vec N & S Concat	0.578±0.040	0.493±0.051	0.562±0.043	0.558±0.042
Graph-level GNN	0.868±0.069	0.494±0.045	0.697±0.113	0.690±0.308

Table 8: AUROC performance on real-world datasets. Standard deviations are provided from runs with 10 random seeds. ‘N’ and ‘S’ stand for ‘Neighborhood’ and ‘Structure,’ respectively.

Method	Datasets			
	PPI-BP	HPO-NEURO	HPO-METAB	EM-USER
SUBGNN (+ GIN)	<b>0.816±0.012</b>	0.862±0.005	<b>0.843±0.014</b>	0.911±0.042
SUBGNN (+ GraphSAINT)	0.797±0.008	<b>0.863±0.011</b>	0.771±0.027	<b>0.947±0.009</b>
Node Averaging	0.498±0.009	0.764±0.104	0.814±0.032	0.896±0.143
Meta Node (GIN)	0.474±0.006	0.516±0.044	0.510±0.036	0.536±0.082
Meta Node (GAT)	0.535±0.017	0.502±0.012	0.581±0.017	0.485±0.056
Sub2Vec Neighborhood	0.518±0.013	0.502±0.014	0.504±0.039	0.496±0.108
Sub2Vec Structure	0.551±0.016	0.498±0.010	0.505±0.016	0.936±0.008
Sub2Vec N & S Concat	0.544±0.011	0.504±0.010	0.496±0.015	0.518±0.048
Graph-level GNN	0.663±0.044	0.773±0.027	0.772±0.018	0.525±0.065

test subgraphs, irrespective of whether the nodes were participating in similar structures or whether the labels between the subgraphs were also shared.

Notably, test subgraphs in the COMPONENT and CORENESS datasets have zero nodes in common with any train or validation subgraphs, yet SUBGNN performs strongly on both datasets (Table 2). Figure 4 shows Micro F1 performance as a function of node overlap on one randomly selected real-world dataset, HPO-METAB. While SUBGNN performs considerably better than majority class and random baselines on the test subgraphs with the smallest percent overlap, it is clear that future research is needed to improve generalization performance.

## Appendix D Implementation Details

**Computing infrastructure.** We leverage Pytorch Geometric (Version 1.4.3) [19] and Pytorch Lightning (Version 0.7.1) [17] for model development. Models were trained on single GPUs from a SLURM cluster containing Tesla V100, Tesla M40, Tesla K80, and GeForce GTX 1080 GPUs.

Table 9: Channel ablation analyses (AUROC). Channels that encode properties relevant to each dataset have a ✓ and best performing channels are in **bold**.

SUBGNN Channel	Datasets			
	DENSITY	CUT RATIO	CORENESS	COMPONENT
Position (P)	0.899±0.016	0.706±0.043	0.712±0.047 ✓	<b>0.997±0.009</b> ✓
Neighborhood (N)	0.904±0.020	0.528±0.078	0.668±0.066	0.955±0.035
Structure (S)	<b>0.971±0.007</b> ✓	<b>0.836±0.021</b> ✓	<b>0.823±0.025</b> ✓	0.834±0.142
All (P+N+S)	0.968±0.008	0.642±0.100	<b>0.824±0.044</b>	0.968±0.032

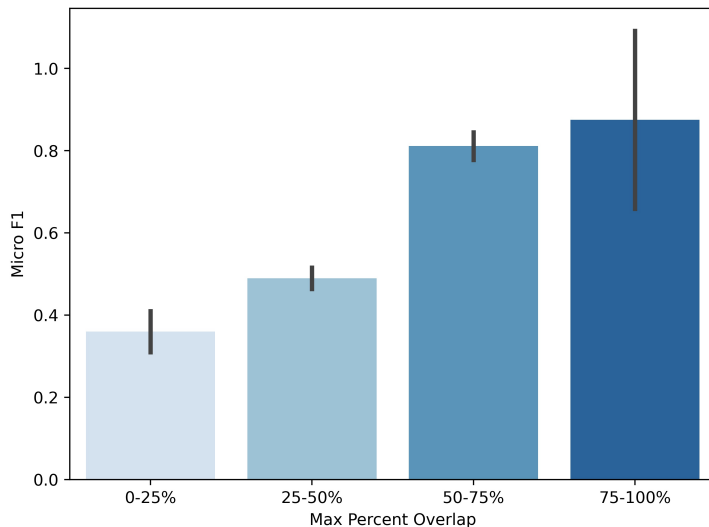


Figure 4: Micro F1 score as a function of maximum percent node overlap with any subgraph in the HPO-METAB train set. Majority class performance = 0.026, and random performance = 0.166. Bars represent standard deviation from runs with 10 random seeds.

**Pretraining node embeddings.** Node embeddings were pretrained using a 2-layer GIN architecture [68]. Hyperparameters were selected from the following ranges: batch size  $\in [256, 4096]$ , learning rate  $\in [5e-3, 5e-5]$ , weight decay  $\in [5e-4, 5e-5]$ , dropout rate  $\in [0.4, 0.5]$ , hidden layer dimension  $\in [128, 512]$ , and output dimension  $\in [32, 128]$ . For all baselines and SUBGNN, we used NEIGHBORSAMPLER [25] in Pytorch Geometric [19] to perform mini-batching with number of hops  $k = 1$  and neighborhood size  $\in [0.1, 1.0]$ . To demonstrate that SUBGNN is not dependent on GIN and NEIGHBORSAMPLER, we replaced the GIN layers with GCN and implemented GRAPHSAINTE for mini-batching given walk length  $\in [16, 32]$  and number of steps  $\in [16, 32]$  [33, 77]. The node features for all graphs were one-hot encodings.

**Model hyperparameter tuning.** Hyperparameters were selected to optimize micro F1 scores on the validation datasets. In the following paragraph, we describe the hyperparameter ranges we explored. The best hyperparameters selected for each model can be found at <https://github.com/mims-harvard/SubGNN>.

Baseline hyperparameters were selected from the following ranges: batch size  $\in [8, 128]$ , learning rate  $\in [1e-5, 0.1]$ , weight decay  $\in [5e-5, 5e-6]$ , and feed forward hidden dimension sizes  $\in [8, 256]$ . For the MN-GAT baseline method, we use the default parameters for GAT, except for the number of heads, which we set to 4. For the S2V-N and S2V-S, methods, we used all of the default parameters in Sub2Vec [2] to train subgraph embeddings; S2V-NS concatenates the resulting embeddings from S2V-N and S2V-S. The GC architecture and hyperparameters were adapted from the Pytorch Geometric GIN example on the MUTAG dataset ([https://github.com/rusty1s/pytorch\\_geometric/blob/master/examples/mutag\\_gin.py](https://github.com/rusty1s/pytorch_geometric/blob/master/examples/mutag_gin.py)) [19].

SUBGNN hyperparameters were selected from the following ranges: batch size  $\in [16, 128]$ , learning rate  $\in [1e-4, 1e-3]$ , gradient clipping  $\in [0, 0.5]$ , number of layers  $l \in [1, 4]$ , k-hop neighborhood  $\in [1, 2]$ , number of internal position anchor patches  $|A_{P_I}| \in [25, 75]$ ,  $|A_{P_B}| \in [50, 200]$ ,  $|A_{N_I}| \in [10, 25]$ ,  $|A_{N_B}| \in [25, 75]$ ,  $|A_S| \in [15, 45]$ , number of LSTM layers  $\in [1, 2]$  with dropout  $\in [0.0, 0.4]$ , and feed forward hidden dimension sizes  $\in [32, 64]$  with dropout  $\in [0.0, 0.4]$ . We additionally experimented with both sum and max aggregation for the connected component initialization from node embeddings, and we tested the Pytorch Lightning auto learning rate finder.

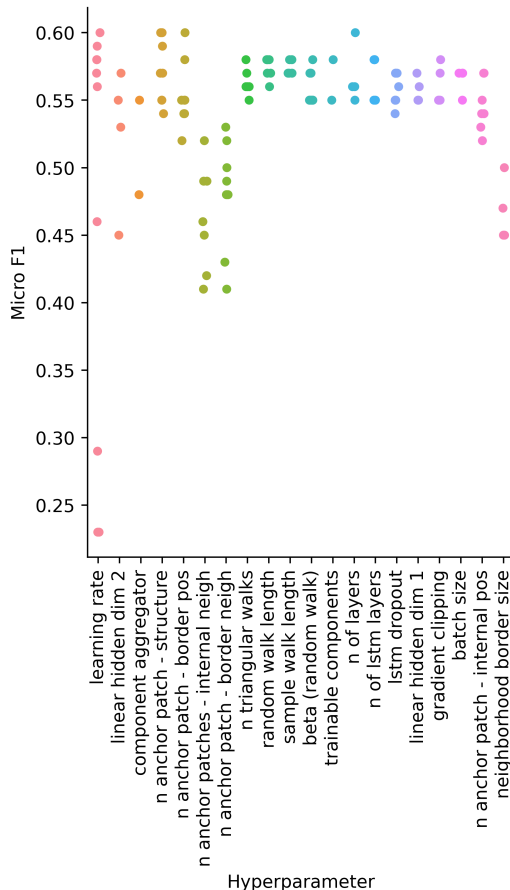


Figure 5: Sensitivity analysis of hyperparameters in SUBGNN. Varying most of the hyperparameters leads to  $< 0.05$  change in Micro F1 score.

## Appendix E Hyperparameter sensitivity analysis

We performed a hyperparameter sensitivity analysis to measure the dependence of SUBGNN on training hyperparameter configuration. Starting with the best performing model for the relevant channel, we vary one hyperparameter at a time and report validation performance on the HPO-METAB dataset. To study model behavior at the extremes, we tested wider hyperparameter ranges: batch size  $\in [16, 128]$ , learning rate  $\in [1e-6, 5e-2]$ , gradient clipping  $\in [0, 1]$ , number of layers  $l \in [1, 4]$ , k-hop neighborhood  $\in [1, 4]$ , number of internal position anchor patches  $|A_{P_I}| \in [1, 100]$ ,  $|A_{P_B}| \in [10, 300]$ ,  $|A_{N_I}| \in [1, 75]$ ,  $|A_{N_B}| \in [1, 150]$ ,  $|A_S| \in [1, 120]$ , number of LSTM layers  $\in [1, 4]$  with dropout  $\in [0.0, 0.8]$ , and feed forward hidden dimension sizes  $\in [8, 256]$ . Of all hyperparameters in our model, we find that seven strongly impact performance (change in micro F1  $> .05$ ), two of which are common across all neural networks: learning rate, feed forward hidden dimension, connected component aggregation (sum or max), number of structure anchors, number of internal and border neighborhood anchors, and number of border position anchors.